PCCP

Cite this: *Phys. Chem. Chem. Phys.*, 2012, **14**, 3381–3387

www.rsc.org/pccp

PAPER

Facile preparation of nitrogen-doped graphene as a metal-free catalyst for oxygen reduction reaction†

Ziyin Lin,[a] Min-kyu Song,[a] Yong Ding,[a] Yan Liu,[a] Meilin Liu[a] and Ching-ping Wong*[ab]

Received 5th January 2012, Accepted 17th January 2012
DOI: 10.1039/c2cp00032f

Nitrogen-doped graphene (nG) is a promising metal-free catalyst for oxygen reduction reaction (ORR) on the cathode of fuel cells. Here we report a facile preparation of nG *via* pyrolysis of graphene oxide with melamine. The morphology of the nG is revealed using scanning electron microscopy and transmission electron microscopy while the successful N doping is confirmed by electron energy loss spectroscopy, Fourier transform infrared spectroscopy, Raman spectroscopy, and X-ray photoelectron spectroscopy. The resulting nG shows high electrocatalytic activity toward ORR in an alkaline solution with an onset potential of −0.10 V *vs.* Ag/AgCl reference electrode. The nG catalyzed oxygen reduction exhibits a favorable formation of water *via* a four-electron pathway. Good stability and anti-crossover property are also observed, which are advantageous over the Pt/C catalyst. Furthermore, the effect of pyrolysis temperature on the structure and activity of nG is systematically studied to gain some insights into the chemical reactions during pyrolysis.

Introduction

The oxygen reduction reaction (ORR) on the cathode of fuel cells still makes considerable contributions to the energy loss in fuel cells. The traditional Pt-based catalyst, developed for Apollo lunar mission in 1960s, exhibits high catalytic activity, and is being continuously optimized in many ways, including tailoring the size-, shape- and alloy-effect.[1–3] However, the high cost and scarcity of Pt intrinsically limit the large scale production and commercialization of Pt-loaded fuel cells. According to the latest cost analysis, Pt-based catalysts account for ~34% of fuel cell stack cost.[4] In addition, the Pt-based catalyst also suffers from crossover and poisoning effects which compromise the efficiency of fuel cells.[5] The search for alternative ORR catalysts has led to the development of many non-precious metal catalysts, including transition metal-microcycles,[6] nano-structured manganese oxides,[7] and metal-free nitrogen-doped carbon materials.[8,9] Recently, it was reported that the nitrogen-doped carbon materials not only have high activity toward ORR, but also long-term durability and tolerance to poisoning. Various forms of nitrogen-doped carbon catalysts have been studied, such as carbon nanotubes,[8] carbon nanofibers,[10] and graphene.[11] Among them, nitrogen-doped graphene (nG) is of particular interest due to the excellent properties of graphene, such as its high surface area and good electrical conductivity.

Chemical vapor deposition (CVD) in the presence of a N source is the most common method for the preparation of nG.[12] However, the growth of nG *via* a CVD method only occurs on the surface of a metal substrate (such as Ni and Cu), and thus is very difficult to scale up. The N atoms can also be incorporated into the graphene lattice by thermally annealing graphene with NH_3,[13] arc discharge of graphite with pyridine/NH_3,[14] and nitrogen plasma treatment of graphene.[15] However, these methods require either toxic gas precursors or special instruments. Moreover, it is difficult to control the type of N functionality in the nG using these methods. It is known that the nature of N functionalities affects the catalytic activity. For example, studies found that the graphitic N is responsible for catalytic activity among various N functionalities.[9,16] Accordingly, it is of great importance to develop a facile method to prepare nG with flexibility to control the type of N functionality.

In this study, we developed a low cost and scalable method for the preparation of nG by thermally annealing graphene oxide (GO) with melamine. As an important derivative of graphene, GO has lots of oxygen-containing moieties on the graphene sheet, providing reactive sites to interact with melamine molecules. Melamine, a common industrial chemical, is chosen as the N source due to its high N content (66.7% by mass), and bi-functional structure where amino groups can interact with

[a] *School of Materials Science and Engineering, Georgia Institute of Technology, 771 Ferst Drive, Atlanta, Georgia 30332, USA. E-mail: cp.wong@mse.gatech.edu; Fax: +1-404-894-9140; Tel: +1-404-894-8391*
[b] *Department of Electronic Engineering, The Chinese University of Hong Kong, Hong Kong*

† Electronic supplementary information (ESI) available: Additional morphological and structural characterizations of nGs; more electrochemical characterizations of nGs and control samples. See DOI: 10.1039/c2cp00032f

GO and triazine rings can be converted to graphitic N. The favorable formation of graphitic N is expected because of the structural similarity between triazine rings and graphitic N. The GO–melamine is pyrolyzed at 400 to 1000 °C to restore the graphene structure with N doping. The evolution of nG structure and the catalytic activity are studied to gain insight into the structure–property relation of nG for ORR.

Experimental

Material synthesis

GO was prepared using the Hummers' method. 50 mg of GO was dispersed in 100 mL of water by sonication. Then 0.25 g of melamine was added into the GO solution which was stirred at 500 rpm until significant agglomeration was observed. The solution was dried at 80 °C in an oven. The solid material was collected and homogenized into fine powders using a mortar and pestle. The GO–melamine powder was pyrolyzed at 400 to 1000 °C for 30 min in an Ar atmosphere to produce nG. Samples are denoted as nG-temperature, where temperate indicates the pyrolysis temperature. The undoped graphene was prepared by pyrolyzing GO at 900 °C for 30 min in an Ar atmosphere, and used as a control sample.

Characterizations

Thermogravimetric analysis (TGA) and differential scanning calorimetry (DSC) were carried out on a simultaneous DSC-TGA analyzer (SDT Q600, TA Instruments Co.). Samples were heated at a rate of 20 °C min^{-1} in nitrogen. Scanning electron microscopy (SEM, LEO 1530) and transmission electron microscopy (TEM, JOEL 100 CX) were used to image the morphology of nGs. Electron energy loss spectroscopy (EELS) was acquired on a Tecnai F30 TEM. Fourier transform infrared spectroscopy (FTIR) characterization was performed at ambient temperature with a FTIR spectrometer (Nicolet, Magna IR 560). Raman characterization was carried out using a LabRAM ARAMIS, Horiba Jobin Yvon, with a 532 nm-wavelength laser. The X-ray photoelectron spectroscopy (XPS) was carried out with a Thermo K-Alpha XPS.

Electrochemical characterizations

The electrochemical properties of nG were tested in a three-electrode system. A Pt wire and Ag/AgCl electrode filled with saturated KCl aqueous solution were used as the counter electrode and reference electrode respectively. The electrolyte was 0.1 M aqueous KOH solution which was purged with nitrogen or oxygen for 10 min prior to the electrochemical test. To prepare the nG-loaded working electrode, nG was dispersed in the mixture of 5 wt% Nafion solution and water (v : v = 1 : 9) by sonication. 10.00 μL of 1 mg mL^{-1} nG dispersion was transferred onto a glassy carbon electrode (GC, 3 mm diameter, 0.07065 cm^2 geometric area) and dried at 80 °C. The nG loading was calculated to be 141 μg cm^{-2}. The control sample of graphene and Pt/C (20 wt% Pt, Alpha Aesar) on GC was prepared in the same way. Cyclic voltammetry (CV) and linear scan voltammetry (LSV) were measured on a Versastat 2-channel system (Princeton Applied Research). The electrocatalytic activities toward ORR were also measured using a rotating disk electrode (Pine Instrument, MSR analytical rotator) at a scan rate of 10 mV s^{-1}. 28 μL of 1 mg mL^{-1} nG dispersion was transferred onto the GC electrode (5 mm diameter, 0.196 cm^2 geometric area) embedded in a PTFE holder, and dried in air at 80 °C for 1 hour. A platinum electrode was used a counter electrode. The 0.1 M KOH solution was prepared as the electrolyte and saturated with oxygen by bubbling with oxygen gas for 30 minutes before measuring ORR activities. The potential was controlled by a potentiostat (Solartron, SI 1286).

Results and discussion

GO is a highly oxidized form of graphene with many O-containing moieties on the surface, such as hydroxyls, epoxies, carbonyls and carboxyls. These O-containing groups are hydrophilic and carboxyls bring in negative charges on the GO surface. As a result, GO can be well dispersed in water, as seen in Fig. S1 (ESI†). After adding melamine, clear agglomeration occurs, indicating a strong interaction between melamine and GO (Fig. S1, ESI†). The nature of GO–melamine interaction could be hydrogen bonding between the amine group in melamine and O-containing groups in GO, ionic bonding between protonated amines and carboxyls, or π–π interaction between unoxidized area in GO and triazine rings.[17,18] The fact that the colloidal GO dispersion is destabilized by adding melamine indicates the existence of ionic bonding that compensates the surface negative charge on GO. The strong interaction between GO and melamine allows the formation of a homogenous GO–melamine composite after drying. As a result, a more efficient doping is expected compared to the previously reported mechanical mixing method.[19]

To monitor the chemical reaction during pyrolysis, the thermal profile of a pyrolyzing GO–melamine mixture was recorded in a SDT in a nitrogen atmosphere. As shown in Fig. 1, the weight loss at ~200 °C is due to the decomposition of labile O-containing groups in GO. There is a significant weight loss between 300–360 °C accompanied by an endothermic peak centered at 348 °C that signifies the sublimation and condensation of melamine. A gradual weight loss is observed between 400–600 °C, possibly due to further condensation of melamine and de-oxygenation of GO. No obvious heat flow is

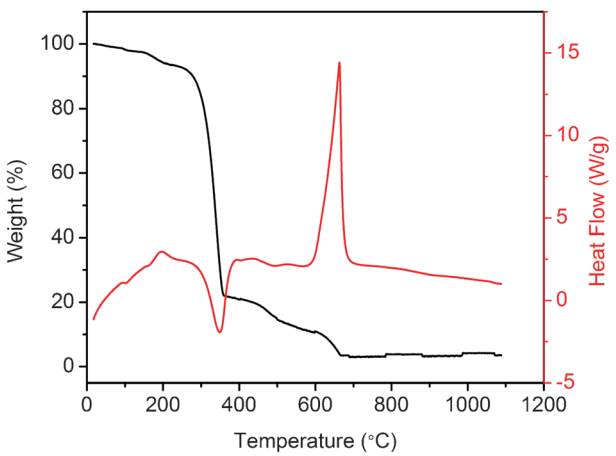

Fig. 1 The SDT profile of GO–melamine in a nitrogen atmosphere at a ramping rate of 20 °C min^{-1}.

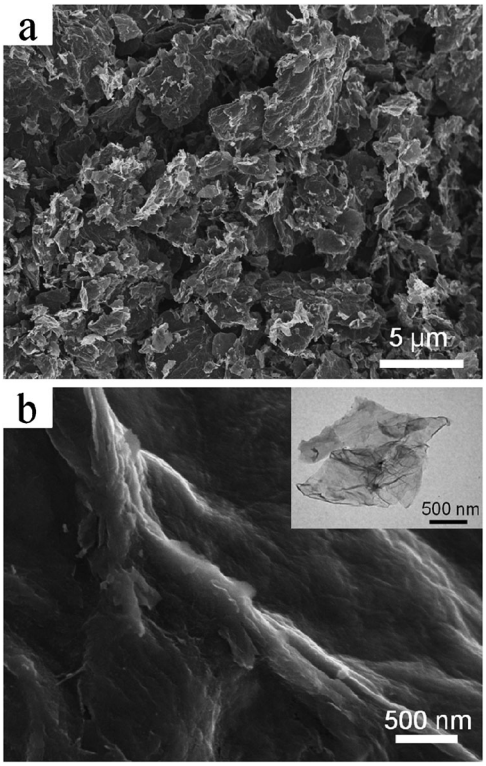

Fig. 2 SEM images of nG-900 at (a) low magnification and (b) high magnification (inset, a TEM image of nG-900).

seen in this temperature range. The complete decomposition of graphitic structure and carbon nitride was observed at ~660 °C with a large exothermic peak. The extensive degradation of carbon nitride is consistent with the previous study on thermal behavior of melamine.[20]

Fig. 2 shows the morphology of nG-900. As seen in the SEM image (Fig. 2a), the nG-900 contains high aspect ratio micron-sized flakes, as well as particles of hundreds of nanometres in size. The flake-like nG-900 is similar to the stacked GO sheets, yet in contrast to pyrolyzed GO which became fully exfoliated at 900 °C (Fig. S2, ESI†). The driving force for GO exfoliation is the high pressure generated by the decomposition of O-containing groups, which produces gaseous molecules faster than their diffusion rate.[21] Exfoliation of GO occurs as soon as this pressure exceeds the van der Waals force between GO sheets.[21] However, after being intercalated with melamine, GO sheets are no longer tightly stacked and thus the high pressure cannot build up. Consequently, no exfoliation is observed for nG-900. Moreover, the zoom-in image shown in Fig. 2b reveals the highly wrinkled nature of nG-900, showing the existence of a significant number of defects. The wrinkles on nG-900 are also observed in TEM (Fig. 2a inset). Interestingly, some holes with diameters of several hundreds of nanometres are observed in both nG-900 (Fig. S3, ESI†) and graphene (Fig. S2, ESI†), possibly due to the loss of carbon atoms during pyrolysis. The existence of holes may be critical to the ORR activity according to a recent computational study.[16]

The N doping in nG-900 could be directly visualized in energy-filtered TEM images. As seen in Fig. 3, a uniform distribution of the N heteroatom on the graphene lattice is observed.

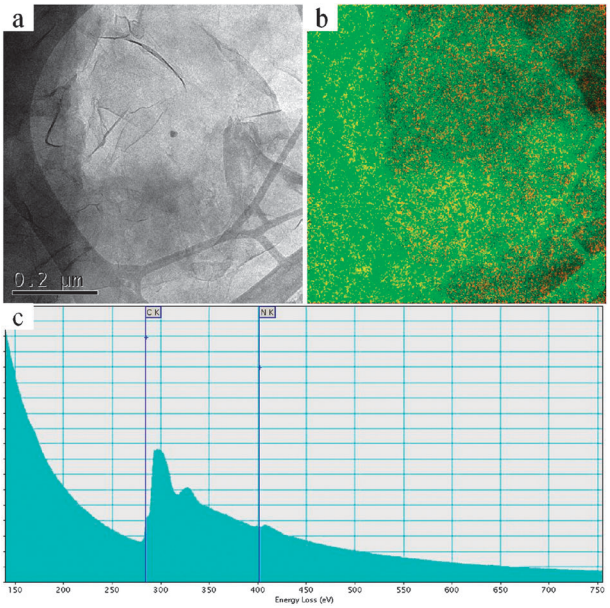

Fig. 3 (a) Bright field TEM image and (b) energy-filtered TEM image of nG-900. Green background and red dots represent C and N respectively. (c) EELS acquired from the area shown in (a).

The N content varies between ~6–9% among different nG-900 sheets. The chemical structure of nG was investigated using FTIR, as shown in Fig. 4a. A complete assignment of peaks is listed in Table S1 (ESI†). In the spectrum of GO, a sharp peak at ~1387 cm^{-1}, a signature for –OH groups, is also present in nG-900, indicating that the hydroxyl is one of the residual O-containing groups in nG-900. Four peaks above 3000 cm^{-1} are found in the spectra of melamine, which could be attributed to $-NH_2$ groups. After pyrolysis at 900 °C, these peaks disappear, indicating a complete removal of amino groups. The elimination of ammonia was reported as a pathway for the condensation of melamine.[20] Furthermore, the peaks at ~1030 and ~810 cm^{-1} are from C–N and triazine rings in melamine and are also seen in the nG-900, evidencing the existence of melamine-like moieties in nG-900. Fig. 4b shows the Raman spectra of GO, graphene and nG-900.

After pyrolysis, the I_D/I_G is 1.0 for GO, and increases to 1.12 for both graphene and nG-900. The increase of I_D/I_G upon GO reduction is normal and could be attributed to the generation of edges and holes observed in SEM images. Furthermore, the G peak position shifts from 1599 cm^{-1} for GO to 1589 cm^{-1} for graphene, indicating the restoration of conjugated structure upon pyrolysis. Interestingly, the G peak of nG-900 further shifts to ~1580 cm^{-1}. The downshift of the G peak in nG is consistent with the previous report, signifying the successful N doping.[12]

The XPS is used as a primary tool to characterize the chemical composition of nG. Fig. 5 shows the XPS spectra of nG-900. The survey spectrum clearly indicates the existence of N in nG-900, estimated to be 8.05%, as well as some residual O-containing groups. The high N content is similar to that determined by EELS. The high resolution C 1 s peak is centered at 284.7 eV, typical for the sp^2 graphitic carbon, and has a tail at higher binding energy as a result of carbon atoms bonded to heteroatoms (O and N). Peak deconvolution is

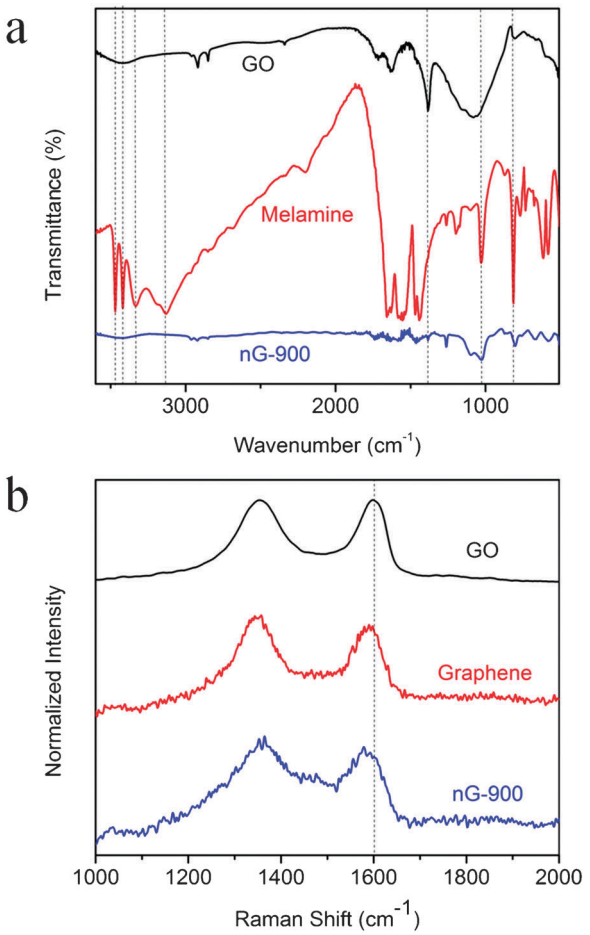

Fig. 4 (a) FTIR spectra of GO, melamine and nG-900 and (b) Raman spectra of GO, graphene and nG-900. The dashed lines indicate the positions of peaks that are specifically discussed.

carried out to fit the C 1 s spectra into four components, which are sp^2 C (284.7 eV), C–O/C═N (286.0 eV), C–N (287.2 eV) and C═O (288.3 eV).[22] It is found that 74.1% C is from graphite structure, 17.9% from C–O/C═N bonds, 6.0% from C–N and 1.9% from C═O bonds. The N 1 s spectrum is very useful for analyzing the nature of N functionalities. Five N-containing groups are possibly present in nGs, which are pyridinic N (N-6), amino N (N–H), pyrolic N (N-5), graphitic N or quaternary N (N–G), and oxygenated N (N–X).[23] The N 1 s spectrum of nG-900 can be deconvoluted into four components at 398.1, 399.6, 401.2, and 403.0 eV, corresponding to N-6, N-5, N–G, and N–X respectively. The percentage of N–G is up to 24.6%, which could be attributed to the structural similarity between melamine and N–G. The existence of N-5, which is not present in precursor melamine, is probably a product of the reaction between GO and amino groups in melamine. Furthermore, the O 1 s spectrum was reasonably fitted into a single peak at 532.1 eV, indicating that hydroxyls, probably in a phenol form, are major O-containing groups in nG-900.[24] This is consistent with the FTIR results. The high thermal stability of phenol was also reported recently.[25]

It is found that the pyrolysis temperature is the primary factor determining the structure of nGs. The evolution of N-containing groups upon pyrolysis is studied by analyzing a series of XPS spectra of nGs. The total N content is obtained from the XPS survey spectrum and plotted in Fig. 6a as a function of pyrolysis temperature. A high N content of 43.0% is found in nG-400, indicating an initial stage of the condensation of melamine and formation of carbon nitride. This is consistent with the SDT profile which gives a temperature of ~348 °C for the sublimation and condensation of melamine. The N content continuously decreases when increasing the temperature to 700 °C, due to further condensation of melamine by deammonation reaction. However, it is found that the N content of nG-700, nG-800 and nG-900 shows similar values of 8.55%, 8.53%, and 8.05%, respectively. The fact that N content does not vary much between 700–900 °C likely results from the finding that at temperatures higher than 700 °C, condensed melamine fully incorporates into the graphitic structure and becomes thermally stable. The incorporation of condensed melamine into graphene, as a dominant pathway for N-doping, is also suggested by control experiments discussed in ESI.† At a higher temperature of 1000 °C, the N content starts to drop to 6.24%.

To study the transformation of N-containing groups during pyrolysis, the percentage of different N-containing groups is obtained from XPS N 1 s spectra and plotted in Fig. 6b.

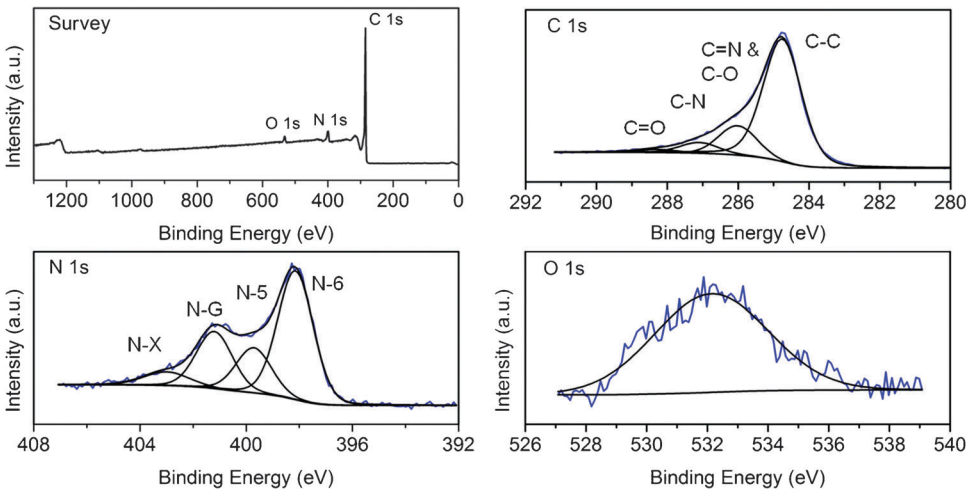

Fig. 5 XPS survey and high resolution C 1 s, N 1 s, O 1 s spectra of nG-900.

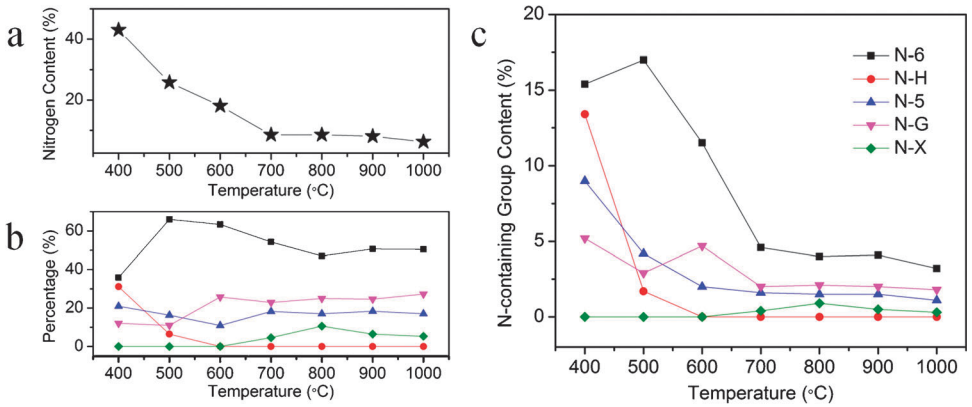

Fig. 6 Evolution of N-containing groups in nGs from XPS characterizations: (a) total N content, (b) percentage of each N-containing group and (c) N-containing group content as a function of pyrolysis temperature. Lines are for visual aid.

It is found that the percentage of N-containing groups shows dramatic changes at temperatures below 700 °C as a result of transformation reactions between different N functionalities, and becomes relatively stable at higher temperatures. The absolute N-containing group content is calculated and shown in Fig. 6c. The following points can be addressed to gain insight into the chemical reactions during pyrolysis: (1) N–H dramatically decreases from 13.4% in nG-400 to 1.7% in nG-500 and disappears at 600 °C and higher, which is consistent with the FTIR result that $-NH_2$ peaks are only observed in nG-400 but not in other nG samples (> 400 °C) (Fig. S4, ESI†). The rapid decrease of N–H confirms that condensation of melamine is through elimination of ammonia, which is completed at temperatures below 600 °C. (2) N-6, a major N-containing group in nG, increases slightly between 400–500 °C, from 15.4% in nG-400 to 17% in nG-500, and meanwhile, N-5 drops from 9% in nG-400 to 1.2% in nG-500. Thus, it is possible that some of N-5 becomes N-6 (or N–G) at 400–500 °C. This is in contrast to previous report that N-5 is stable until 600 °C.[23] (3) The percentage of N functionalities in nG, especially the high content of N–G, is significantly different from typical carbon nitride prepared from melamine,[26] confirming that N is effectively doped into the graphitic lattice instead of forming carbon nitride clusters on graphene. The above information about the transformation of N functionalities during pyrolysis provides guidelines for further studies on the preparation of nG,

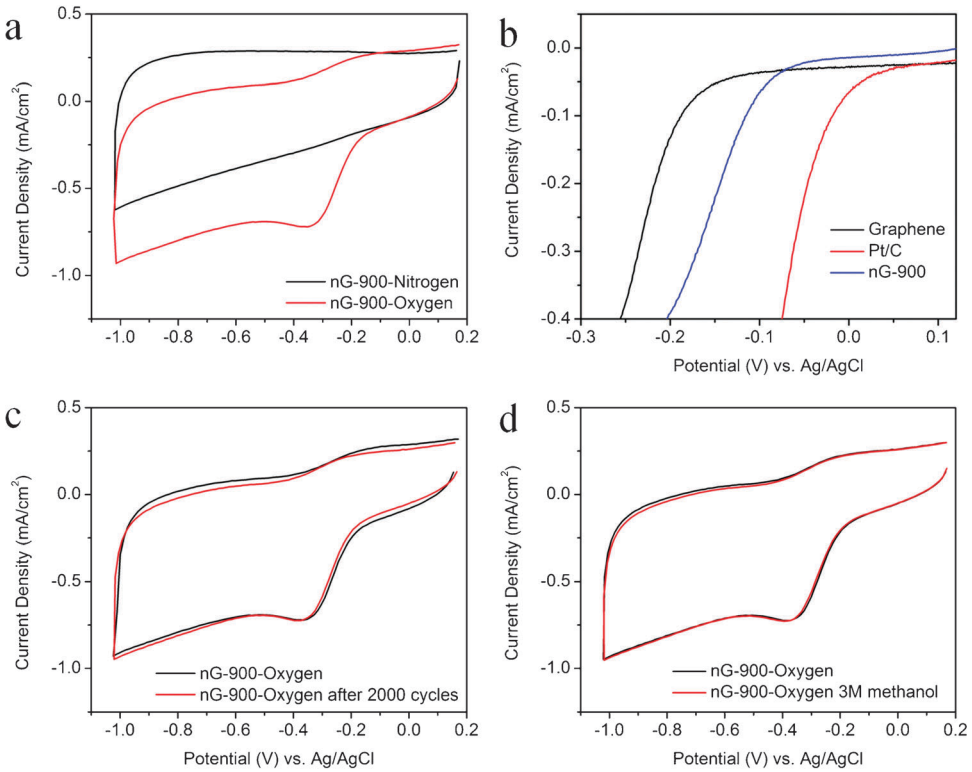

Fig. 7 Electrochemical characterizations of nG-900: (a) CVs in 0.1 M KOH at a scan rate of 100 mV s^{-1}; (b) LSVs of graphene, nG-900 and Pt/C in 0.1 M oxygen saturated KOH at a scan rate of 10 mV s^{-1}; (c) CVs of nG-900 before and after the stability test (2000 cycles in oxygen saturated 0.1 M KOH at a scan rate of 100 mV s^{-1}); (d) CVs of nG-900 with and without 3 M methanol.

such as the use of different N-containing precursors (urea, polyaniline, polypyrrole, *etc*).

The catalytic activity of nG was first examined using CV in the nitrogen or oxygen saturated 0.1 M KOH solution. Fig. 7a shows a typical CV for nG-900. In nitrogen saturated KOH, a featureless capacitive current background was observed between −1.0 and 0.2 V. After introducing oxygen, a large cathodic current with a peak at −0.34 V is clearly observed, evidencing the catalytic activity of nG-900 toward ORR. The onset potential of oxygen reduction is an important criterion to evaluate the activity of ORR catalyst, which was measured by LSV. As seen in Fig. 7b, nG-900 exhibits an onset potential of −0.10 V. In comparison, the graphene control sample has an onset potential of −0.19 V, and the state-of-art Pt/C catalyst shows higher activity with an onset potential of −0.03 V. However, the advantage of nG-900 over Pt/C is clearly seen in the stability and crossover tests. As seen in Fig. 7c, after 2000 CV cycles, nG-900 shows a negligible degradation, while Pt/C has a significant loss in activity (Fig. S5a, ESI†) as a result of possible migration, dissolution or aggregation of Pt nanoparticles. The excellent stability of nG could be attributed to the stable covalent bond between the active site at the graphitic lattice in nG-900. Moreover, the addition of 3 M methanol, a common fuel in fuel cells, does not change the CV of nG-900 significantly (Fig. 7d). In contrast, obvious methanol oxidation occurs on Pt/C as seen in Fig. S5b (ESI†), which will lower the efficiency of fuel cells. The ORR reaction on nG is also studied by RDE, as seen in Fig. 8. The number of electrons transferred per oxygen molecule is calculated by Koutecky–Levich equations (Fig. S6, ESI†), and found to be 3.3–3.7 at potentials ranging from −1 to −0.3 V (Fig. 8 inset). This suggests that the ORR catalyzed by nG-900 is dominated by a one-step four-electron pathway producing water molecules.

The catalytic activity of nG is highly dependent on the pyrolysis temperature which is related to the competition between N content and electrical conductivity. As seen in Fig. S7 (ESI†), nG-400 and nG-500 show onset potentials at −0.25 and −0.21 V respectively. Their limited catalytic activities, although with high N content, could be attributed to the existence of a significant amount of electrically insulating carbon nitride. As a result, electrons cannot effectively propagate through the carbon nitride/nG structure. The low electrical conductivity of nG-400 and nG-500 is revealed by the negligible capacitive backgrounds in their CVs (Fig. S8, ESI†). The removal of carbon nitride at higher temperature leads to an improved electrical conductivity and thus an enhanced capacitive current background (Fig. S8, ESI†). The onset potentials of nGs (> 600 °C) shift positively as a consequence. However, once the pyrolysis temperature is higher than 900 °C, the N content decreases, resulting in a slightly lower activity for nG-1000 (Fig. S7, ESI†).

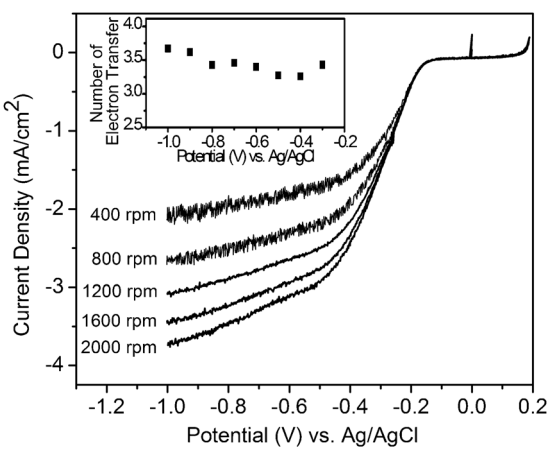

Fig. 8 RDE measurement of nG-900 in 0.1 M oxygen saturated KOH at a scan rate of 10 mV s^{-1}; inset: the number of electrons transferred as a function of potential.

Conclusions

We have developed a simple method for effective doping of N atoms into the graphene lattice by pyrolyzing GO with melamine. The morphology, structure and composition of nG are characterized using electron microscopy (SEM and TEM) and spectroscopy (EELS and XPS) as well as vibrational spectroscopy (FTIR and Raman). The total N content in nG is up to 8.05% with a high percentage of graphitic N that is believed to be vital to the catalytic activity toward ORR. Electrochemical tests of nG-900 show high catalytic activity toward ORR with good stability and resistance to crossover. Moreover, the evolution of catalytic activity with the pyrolysis temperature is discussed on the basis of the structural information obtained from the XPS study, which provides insight into the structure–property relation of the nG as an ORR catalyst.

Acknowledgements

The authors would like to acknowledge the financial support from Natural Science Foundation (NSF, 0800849).

Notes and references

1 V. R. Stamenkovic, B. Fowler, B. S. Mun, G. F. Wang, P. N. Ross, C. A. Lucas and N. M. Markovic, *Science*, 2007, **315**, 493–497.
2 Z. Y. Lin, H. B. Chu, Y. H. Shen, L. Wei, H. C. Liu and Y. Li, *Chem. Commun*., 2009, 7167–7169.
3 S. Mukerjee, *J. Appl. Electrochem*., 1990, **20**, 537–548.
4 B. James, J. Kalinoski and K. Baum, http://www.hydrogen.energy.gov/pdfs/review10/fc018_james_2010_o_web.pdf.
5 M. Winter and R. J. Brodd, *Chem. Rev*., 2004, **104**, 4245–4269.
6 M. Lefevre, E. Proietti, F. Jaouen and J. P. Dodelet, *Science*, 2009, **324**, 71–74.
7 F. Y. Cheng, Y. Su, J. Liang, Z. L. Tao and J. Chen, *Chem. Mater*., 2010, **22**, 898–905.
8 K. P. Gong, F. Du, Z. H. Xia, M. Durstock and L. M. Dai, *Science*, 2009, **323**, 760–764.
9 R. L. Liu, D. Q. Wu, X. L. Feng and K. Mullen, *Angew. Chem., Int. Ed*., 2010, **49**, 2565–2569.
10 S. Maldonado and K. J. Stevenson, *J. Phys. Chem. B*, 2005, **109**, 4707–4716.
11 L. T. Qu, Y. Liu, J. B. Baek and L. M. Dai, *ACS Nano*, 2010, **4**, 1321–1326.
12 D. C. Wei, Y. Q. Liu, Y. Wang, H. L. Zhang, L. P. Huang and G. Yu, *Nano Lett*., 2009, **9**, 1752–1758.
13 X. R. Wang, X. L. Li, L. Zhang, Y. Yoon, P. K. Weber, H. L. Wang, J. Guo and H. J. Dai, *Science*, 2009, **324**, 768–771.
14 L. S. Panchokarla, K. S. Subrahmanyam, S. K. Saha, A. Govindaraj, H. R. Krishnamurthy, U. V. Waghmare and C. N. R. Rao, *Adv. Mater*., 2009, **21**, 4726–4730.
15 Y. Wang, Y. Y. Shao, D. W. Matson, J. H. Li and Y. H. Lin, *ACS Nano*, 2010, **4**, 1790–1798.

16 T. Ikeda, M. Boero, S. F. Huang, K. Terakura, M. Oshima and J. Ozaki, *J. Phys. Chem. C*, 2008, **112**, 14706–14709.
17 Z. Y. Lin, Y. Liu and C. P. Wong, *Langmuir*, 2010, **26**, 16110–16114.
18 J. D. Wuest and A. Rochefort, *Chem. Commun.*, 2010, **46**, 2923–2925.
19 F. B. Wang, Z. H. Sheng, L. Shao, J. J. Chen, W. J. Bao and X. H. Xia, *ACS Nano*, 2011, **5**, 4350–4358.
20 L. Costa and G. Camino, *J. Therm. Anal.*, 1988, **34**, 423–429.
21 M. J. McAllister, J. L. Li, D. H. Adamson, H. C. Schniepp, A. A. Abdala, J. Liu, M. Herrera-Alonso, D. L. Milius, R. Car, R. K. Prud'homme and I. A. Aksay, *Chem. Mater.*, 2007, **19**, 4396–4404.
22 D. Marton, K. J. Boyd, A. H. Albayati, S. S. Todorov and J. W. Rabalais, *Phys. Rev. Lett.*, 1994, **73**, 118–121.
23 J. R. Pels, F. Kapteijn, J. A. Moulijn, Q. Zhu and K. M. Thomas, *Carbon*, 1995, **33**, 1641–1653.
24 C. A. Ventrice, D. Yang, A. Velamakanni, G. Bozoklu, S. Park, M. Stoller, R. D. Piner, S. Stankovich, I. Jung, D. A. Field and R. S. Ruoff, *Carbon*, 2009, **47**, 145–152.
25 A. Ganguly, S. Sharma, P. Papakonstantinou and J. Hamilton, *J. Phys. Chem. C*, 2011, **115**, 17009–17019.
26 X. F. Li, J. Zhang, L. H. Shen, Y. M. Ma, W. W. Lei, Q. L. Cui and G. T. Zou, *Appl. Phys. A: Mater. Sci. Process.*, 2009, **94**, 387–392.